JACS
JOURNAL OF THE AMERICAN CHEMICAL SOCIETY

Article

pubs.acs.org/JACS

Nature and Structure of Aluminum Surface Sites Grafted on Silica from a Combination of High-Field Aluminum-27 Solid-State NMR Spectroscopy and First-Principles Calculations

Rachel Nathaniel Kerber,[†] Anthony Kermagoret,[‡] Emmanuel Callens,[‡,§] Pierre Florian,[⊥] Dominique Massiot,[⊥] Anne Lesage,[∥] Christophe Copéret,*[,‡,⊗] Françoise Delbecq,[†] Xavier Rozanska,[†,▽] and Philippe Sautet*[,†]

[†]Université de Lyon, CNRS, Institut de Chimie de Lyon, Ecole Normale Supérieure de Lyon, 46 allée d'Italie, F-69364 Lyon Cedex 07, France

[‡]Laboratoire de Chimie Organométallique de Surface, CNRS, UMR 5265 C2P2, Université Lyon 1, CPE Lyon, France

[§]KAUST Catalysis Center, King Abdullah University of Science and Technology, P.O. Box 55455, Jeddah 21534, Saudi Arabia

[⊥]CEMHTI CNRS UPR3079, Université d'Orléans, 1D Avenue de la Recherche-Scientifique, F-45071 Orléans Cedex 2, France

[∥]Université de Lyon, Centre de RMN à Très Hauts Champs, CNRS, Ecole Normale Supérieure de Lyon, UCB-Lyon 1, 5 rue de la Doua, F-69100 Villeurbanne, France

Supporting Information

ABSTRACT: The determination of the nature and structure of surface sites after chemical modification of large surface area oxides such as silica is a key point for many applications and challenging from a spectroscopic point of view. This has been, for instance, a long-standing problem for silica reacted with alkylaluminum compounds, a system typically studied as a model for a supported methylaluminoxane and aluminum cocatalyst. While ^{27}Al solid-state NMR spectroscopy would be a method of choice, it has been difficult to apply this technique because of large quadrupolar broadenings. Here, from a combined use of the highest stable field NMR instruments (17.6, 20.0, and 23.5 T) and ultrafast magic angle spinning (>60 kHz), high-quality spectra were obtained, allowing isotropic chemical shifts, quadrupolar couplings, and asymmetric parameters to be extracted. Combined with first-principles calculations, these NMR signatures were then assigned to actual structures of surface aluminum sites. For silica (here SBA-15) reacted with triethylaluminum, the surface sites are in fact mainly dinuclear Al species, grafted on the silica surface via either two terminal or two bridging siloxy ligands. Tetrahedral sites, resulting from the incorporation of Al inside the silica matrix, are also seen as minor species. No evidence for putative tri-coordinated Al atoms has been found.

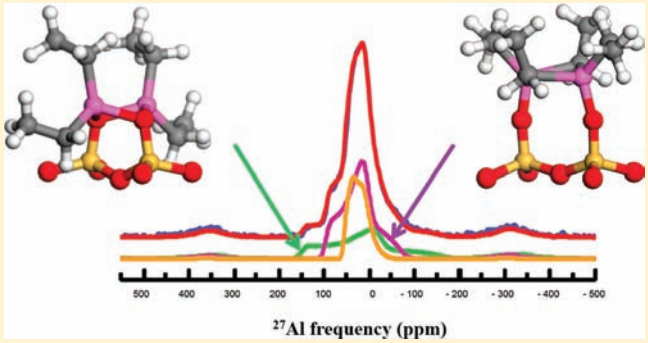

INTRODUCTION

The chemistry of oxide surfaces is a topic of major interest for a wide range of applications in materials science and chemistry. A key challenge is to determine the nature and the structure of the oxide termination, since this controls most properties, including chemical reactivity.[1−5] In many cases, the surface will be postmodified by a chemical treatment in order to generate sites with specific properties (electronic, magnetic, chemical). One of the objectives, for example, is to generate sites with strong Lewis acidity by introducing main-group elements such as Al or B in low coordination at the surface of solid oxides, thus allowing the tuning of their catalytic reactivity for numerous industrial processes.[6−9]

In that respect, aluminum species supported or not on oxide or oxide-modified supports have generated many debates in the literature; this is especially the case for methylaluminoxane (MAO) and its supported version.[10] Indeed, MAO is by far the most efficient co-catalyst for olefin polymerization or oligomerization catalytic systems,[11,12] but its structure, active sites, and activation mechanism remain largely unknown.[11,13−16] Grafted on various oxide supports,[17−19] MAO led to poor cocatalytic activity in various heterogeneous oligomerization catalytic systems, and it thus requires using very high Al/metal ratio.[10,20,21]

To determine and to mimic the active sites of supported MAO, several methods have been developed, for instance via grafting trimethylaluminum (TMA) on silica supports.[22−26] However, the surface chemistry of alkylaluminum species is quite complex: it can involve grafting on surface OH groups, or

Received: January 26, 2012
Published: March 22, 2012

   dx.doi.org/10.1021/ja3008566 | J. Am. Chem. Soc. 2012, 134, 6767−6775

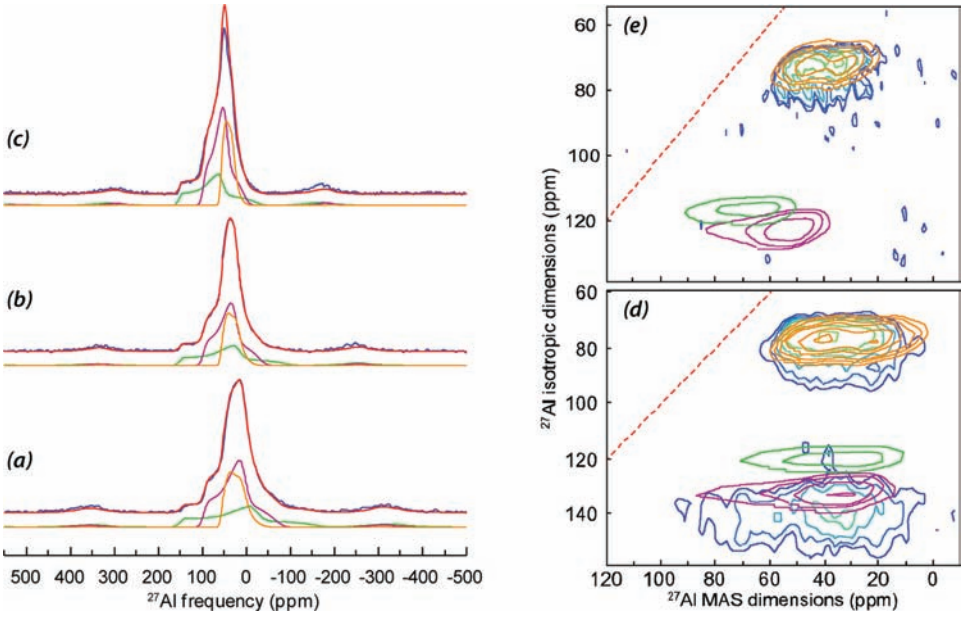

Figure 1. ^{27}Al NMR experiments. One-dimensional full-echo spectra (blue line) obtained at 17.6 (a), 20.0 (b), and 23.5 T (c), along with the three-component simulation (in green, pink, and yellow lines) and the resulting line shape (red line). MQMAS spectra (blue) at 20.0 (d) and 23.5 T (e), with the expected positioning of those three components.

possibly on siloxane bridges, as well as the reconstruction of the silica surface via alkyl transfer on adjacent siloxane bridges, which is evidenced by the formation of $MeSi(O)_3$, $(Me)_2Si(O)_2$, and $(Me)_3SiO$ species.[26−28] This indeed implies the presence of various possible surface coordinations for aluminum atoms in monomeric or oligomeric forms, in particular the speculated presence of highly reactive tricoordinated Al(III) species.[24] However, to date, there is no direct spectroscopic evidence for the structure of the surface Al species, and their identification has remained a challenge.[24,27]

A method of choice to understand Al sites at a molecular level could be aluminum-27 solid-state NMR spectroscopy, as reported for Al sites on alumina.[29] However, field-dependent line broadening due to large second-order quadrupolar interaction effects usually makes the acquisition and interpretation very complex for such materials.[30,31]

Here we combine the acquisition of spectra at the highest available principal fields (17.6, 20.0, and 23.5 T) and ultrafast magic angle spinning (MAS, >60 kHz)[32,33] to determine the nature and the structure of the Al surface sites when triethylaluminum (TEA) is reacted with mesoporous silica SBA-15, taken as a model system presenting various aluminum sites. The NMR parameters {quadrupolar coupling constant (C_Q), isotropic chemical shift (δ_{iso}), and asymmetry parameter (η_Q) of the electric field gradient tensor (EFG)} are extracted from a consistent modeling of all the spectra acquired at different fields, taking into account disorder effects. In parallel, a large number of potential Al sites on silica have been screened by first-principles calculations, combining cluster models and periodic approaches and calculating their optimal geometry and their NMR parameters. The surface structure is obtained by a direct comparison of the NMR parameters extracted from the spectra and those calculated from first principles.

We here benefit from the fact that quadrupolar nuclei are very sensitive to their environment through their NMR parameters.[34−36] These NMR parameters constitute indeed a real signature for aluminum species.[30]

This combination of approaches clearly shows that Al species are not present in the form of monomers but as Al dimers with a tetrahedral environment for the Al atoms on the silica surface. Two specific structures for these dimers are associated with two sites in the NMR experimental analysis. In addition, Al atoms, after multiple alkyl transfers, can be incorporated in the silica lattice, in association with the third experimental component.

RESULTS AND DISCUSSION

Reaction of TEA in hexane/pentane solution (3 equiv/silanol) with SBA-15[37] (previously dehydroxylated at 500 °C under very high vacuum, specific surface of 690 $nm^2 \cdot g^{-1}$, and OH coverage (θ_{OH}) = 1.3−1.4 nm^{-2}) for 1 h at 25 °C led to the formation of ∼1 equiv of ethane per surface OH group (1.28 ethane·nm^{-2}), consistent with the reaction of all OH groups.[38] Elemental analysis on the resulting solid showed an aluminum loading of 5.69 wt %, which corresponds to 2.3 Al atoms per nm^2 (Al/SiOH ratio of 1.8), and a carbon loading of 11.62 wt %, showing a C/Al ratio of 4.6. These data suggest the formation of dimeric Al surface complexes and/or reaction with siloxane bridges in place of OH. A simple protonolysis of one Et−Al bond of Et_3Al would lead to 1Al/OH and 4C/Al, the attachment of dimeric species by simple protonolysis to 2Al/OH, 5C/Al. Diffuse reflectance IR spectroscopy (DRIFT) of the solid confirmed that all silanols were consumed upon grafting, leading to the appearance of the characteristic vibrations for surface alkyl groups with C−H stretching and bending vibrations observed in the 3000−2850 and 1500−1350 cm^{-1} regions, respectively (Supporting Information Figure S1).[39] Carbon-13 CP-MAS solid-state NMR spectroscopy (Figure S2) showed the presence of two main signals, one at 0.2 ppm, attributed to Al-CH_2, and one at 6.5 ppm, which can be assigned to -CH_3 as well as Si-CH_2 signals (vide infra).[40] Finally, the silicon-29 solid-state NMR spectrum of TEA@SBA-15 presented four signals at −107.4, −57.2, −8.7, and 26.6 ppm, attributed to $Si(O)_4$, $EtSi(O)_3$, $(Et)_2Si(O)_2$, and $(Et)_3SiO$, respectively (Figure S2). These $(Et)_xSi(O)_{4-x}$ species

dx.doi.org/10.1021/ja3008566 | J. Am. Chem. Soc. 2012, 134, 6767−6775

clearly show that siloxane bridges are involved in the grafting process, probably via transfer of alkyl groups from surface alkylaluminum species to adjacent Si atoms by cleavage of Si−O−Si bridges of the silica support (eq 1).[27,28]

$$X_2Al—R + \equiv Si—O—Si\equiv \rightarrow Si—O—AlX_2 + \equiv Si—R \quad (1)$$

High Magnetic Field Aluminum-27 Solid-State NMR Spectroscopy. The ^{27}Al spectra acquired at three different high fields, namely 17.6, 20.0, and 23.5 T (Figure 1), under ultrahigh MAS (>60 kHz) show broad central transitions sharpening with increasing magnetic fields, indicative of a dominant contribution of the second-order quadrupolar broadening, which is proportional to the inverse of the squared magnetic field when expressed in ppm, where effects of the distribution of chemical shift remain constant. Low-intensity spinning side bands clearly indicate that the combination of high magnetic fields and high-speed spinning rates does allow most of the intensity to be located in the $N = 0$ spinning side bands. Both spectra clearly show marked inflection points that are linked to the discontinuities of the second-order quadrupolar line shapes, smoothed by a distribution of quadrupolar interactions and isotropic chemical shifts. They also indicate that a purely statistical disorder model such as the Gaussian isotropic model (Czjzek, $d = 5$)[41] used for accounting for ^{27}Al spectra in glasses cannot be used in that case.[42] The extended Czjzek model, recently described by Le Caër and co-workers,[43] allows drawing a continuous evolution between a perfectly defined site (defined by C_Q and η_Q) and a statistical disorder and has thus been applied in the modeling of the observed spectrum.[44,45]

The simulation is first performed simultaneously for the two 1D data sets obtained at 17.6 and 20.0 T (i.e., on the exact same sample, not removed from the rotor), and the agreement is excellent when taking into account three contributions (Figure 1a and b). The positions of the discontinuities are well rendered, and the relative intensities are identical for the two spectra. Small discrepancies can be attributed to the model's limitations and in particular to the fact that the chemical shift anisotropy is not taken into account. Using this exact set of parameters, we simulated the spectra obtained at 23.5 T on a "fresh" sample; as seen from Figure 1c, it leads to a close-to-perfect agreement. The very slight discrepancy in the intensities is due to the extremely high sensitivity of this compound to oxidation, affecting the relative proportion of sites. This ensemble of experiments leads overall to the very reliable set of NMR parameters listed in Table 1. The site **S1** (in green, Figure 1) with (δ_{iso} [ppm], C_Q [MHz]) of (154 ppm, 27.3 MHz) accounts for the sharp discontinuity located around 150 ppm and the trailing intensity between −100 and −150 ppm. The other marked discontinuity seen around 100 ppm is taken into account by the site **S2** (98 ppm, 19.9 MHz), which also produces the inflection point seen at −50 ppm (in pink, Figure 1). Those two components have rather well-defined second-order quadrupolar line shapes, evidencing a small distribution of quadrupolar parameters and hence pointing to rather well-defined chemical species. This is in contrast with the third component **S3** (in yellow, Figure 1), which is significantly broadened, as seen from its high value of ΔC_Q.

Table 1. ^{27}Al NMR Parameters[a] Accounting for the Experimental Spectrum

site	δ_{iso} (ppm)	$\Delta\delta_{iso}$ (ppm)	C_Q (MHz)	ΔC_Q (MHz)	η_Q	ε	intensity (%)
S1	154	5.1	27.3	1.75	0.80	0.10	28
S2	98	14.2	19.9	1.44	0.80	0.15	47
S3	60	7.9	15.1	2.85	0.40	0.15	25

[a] δ_{iso}, average isotropic chemical shift; $\Delta\delta_{iso}$, fwhm of the Gaussian distribution of chemical shift; C_Q, average quadrupolar coupling; ΔC_Q, fwhm of the equivalent distribution of quadrupolar coupling; η_Q, asymmetry parameter of the base quadrupolar tensor; ε, epsilon factor of the extended distribution.[43]

Despite the intrinsic lack of sensitivity of ^{27}Al in this sample (already 1 day acquisition of 1D experiment) and large quadrupolar couplings, we were able to perform multi-quantum (MQ) MAS experiments at 20.0 T (3 days) and 23.5 T (2 days) to ascertain the validity of the proposed decomposition, taking advantage of the high radio frequency (rf) fields available in the 1.3 mm MAS probe. The spectra at 20.0 and 23.5 T are shown in Figure 1d and e. The parameters listed in Table 1 account perfectly for the third site (60 ppm, 15.1 MHz), which is clearly seen in both MQMAS experiments since its "small" quadrupolar coupling constant allows efficient triple-quantum excitation. Although much lower in intensity, the second (98 ppm, 19.9 MHz) site is visible at $\delta_1 \approx 140$ ppm in the indirect dimension of the 20.0 T experiment, and its fitted NMR parameters fairly well reproduce this position. Much longer acquisition time (and slightly higher rf field) would be needed to observe such a signal even at 23.5 T. According to the 1D simulation, the first (154 ppm, 27.3 MHz) site should show up around $\delta_1 \approx 220$ ppm, but since we used a small indirect spectral width (to maximize the signal-to-noise ratio), it would be folded around $\delta_1 \approx 120$ ppm, i.e., between the two other contributions. There is clearly no signal at that position, and the very large quadrupolar coupling of this component is likely preventing us from observing it in this type of experiment. Overall, these MQMAS experiments support the validity of the NMR parameters obtained from the simultaneous simulation of the two spectra obtained at 17.6 and 20.0 T. Moreover, the 1D and 2D experiments together allow the estimation of the following uncertainties: δ_{iso} ±2 ppm, C_Q ±0.5 MHz, and ΔC_Q ±0.7 MHz.

Nature of Surface Species. While the determination of the structure of the Al surface species is crucial to understand the potential surface reactivity, it is, however, highly challenging to attribute the NMR signals to a specific species because of the numerous potential $(Alk)_nAl(O)_m$ molecular structures (Scheme 1).[46−50] Grafting alkylaluminum compounds on silica partially dehydroxylated at 500 °C can be decomposed in two steps. Protonolysis on surface OH groups should first mainly yield the expected mono-siloxy surface species, even if bis-grafted species via reaction of two surface silanols per Et_3Al and in particular Et_6Al_2 should not be ruled out. Additionally, formation of dimeric species is also possible through μ^2-Et or O ligands, as typically observed for aluminum compounds.[51,50−54] In fact, TEA is dimeric in solution.[55] In a second step, after grafting on surface silanols, the aluminum center must also undergo further reaction with adjacent Si−O−Si bridges via multiple alkyl transfers, as evidenced by the presence of $AlkSi(OSi)_3$, $(Alk)_2Si(OSi)_2$, and $(Alk)_3SiOSi$ species (Supporting Information Figure S2, see also literature precedents).[22,24,27,56−59] It is thus possible to propose several possible grafted aluminum species.

First-Principles Simulations. According to these various coordination modes and possible rearrangements, the structure

dx.doi.org/10.1021/ja3008566 | J. Am. Chem. Soc. 2012, 134, 6767−6775

Scheme 1. Possible Surface Species Resulting from Reaction of Triethylaluminum with a Silica Surface: (a) Reaction of Et_3Al and/or Its Dimer with a Surface Silanol; (b) Examples of Possible Bis-grafted Species; (c) Examples of Ethyl Transfer Processes Leading to the Formation of $(Et)_xSi(O)_{4-x}$ Surface Species (x = 1, 2, and 3)

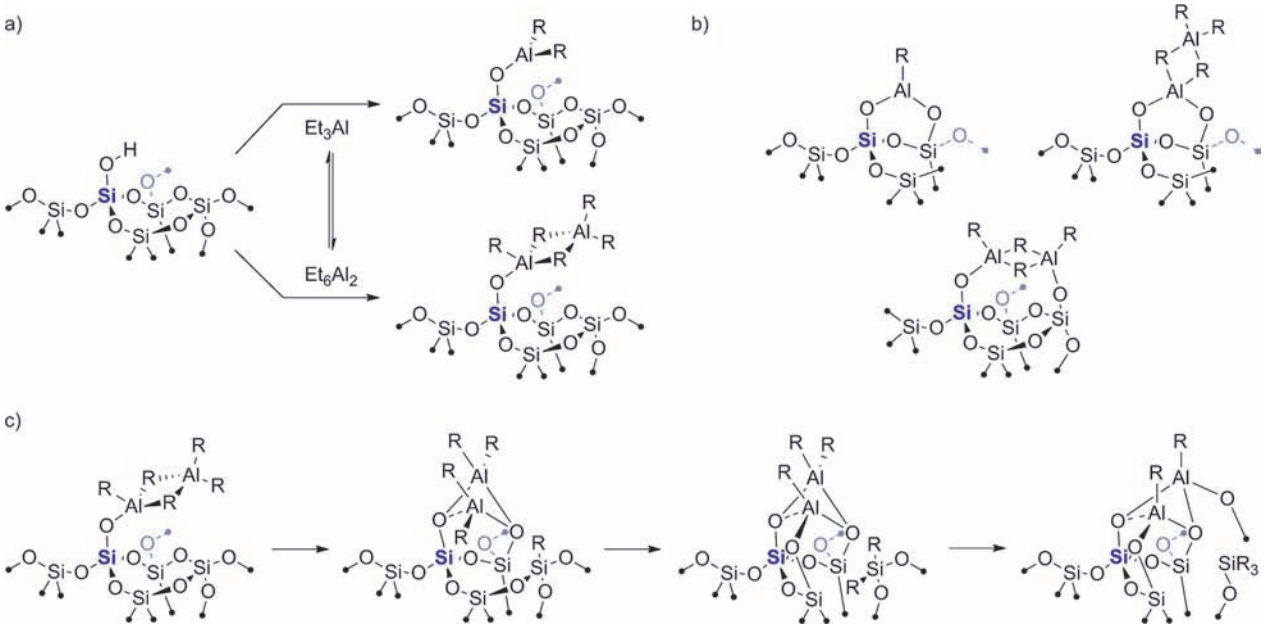

and energy of grafted Al species together with their associated NMR properties (in particular C_Q and δ_{iso}, which are very sensitive to the local environment of Al, vide infra) were investigated by DFT calculations by combining cluster and periodic slab models for silica (Figure 2). The cluster models allow representing generic environments for the Al centers as monomers (**MX** and **MX**^{S}) or dimers (**DX.Y** and **DX.Y**^{S}), including all the dimers proposed in Scheme 1. **M** stands for monomer and **D** stands for dimer, with **X** corresponding to the number of O atoms interacting with the Al species and **Y** discriminating between different types of grafted dimers. **S** denotes structures with Si−O−Si connections between the Si centers, hence modeling surface sites. Structural optimization of these various models is followed by calculation of the C_Q, δ_{iso}, and η_Q NMR parameters. For our purpose, it is important to determine the error bar in these DFT NMR calculations. This was performed with test calculations on well-defined Al-containing molecules and solids, showing a good agreement between calculated and experimental NMR parameters, with differences below 2 MHz for C_Q, 10 ppm for δ_{iso}, and 0.3 for η_Q (see Supporting Information and Table S1). Our structural study will hence be primarily based on C_Q and δ_{iso}.

The calculated NMR parameters are given in Table 2 and compared to those for the isolated TEA monomer, Et_3Al, and dimer, Et_6Al_2. First, all tricoordinated monomeric species **M1**−**M3** show very high C_Q values (ranging between 42 and 37 MHz with C_Q = 47 MHz for isolated monomeric Et_3Al), with none of them matching experimental values. It is noteworthy that substitution of each Et by a O−Si(OH)$_3$ ligand decreases the C_Q and δ_{iso} values.

Second, all dimeric species have tetracoordinated Al centers and hence lower C_Q values than tricoordinated Al. The C_Q parameter for the isolated dimer (23 MHz) does not correspond to any experimental value. Upon chemical grafting, in this case, the trend for the substitution of Et by siloxy ligands [O−Si(X)$_3$] is more complex, and the position of the O substitution in the dimeric structures, terminal (μ^1) or bridging (μ^2), has a dramatic influence. Compared to the case of the Et_6Al_2 dimer, a surface species with a terminal siloxy ligand (**D1.1**) results in a significant decrease of C_Q and δ_{iso} for the Al site containing the siloxy ligand, as was the case for the monomer, while the NMR parameters for the other Al site, keeping four alkyl ligands, are weakly affected. A dimeric species with each Al center having a terminal siloxy group (**D2.1**) restores two equivalent Al sites. In contrast, the bridging oxygen coordination (**D1.2**) gives no decrease of the NMR parameters and even a slight increase of C_Q compared to that for Et_6Al_2. Species with two bridging μ^2-siloxy groups (**D2.2** and **D2.2**^{S}) show a further increase of C_Q. The NMR parameters are hence not simply correlated with the nature of the ligands around the Al centers—with the bridging ligands playing a specific role. The angular deformation from **D2.2** to **D2.2**^{S} induced by the formation of the Si−O−Si bridge is important, but the geometry around the Al atoms is only weakly affected (Al−O and Al−C distances unchanged; angles around Al modified by less than 6°), and the NMR parameters do not significantly change. This implies that the calculated NMR data are only weakly dependent on details on the silica surface, such as the separation of Si−O groups in cases where two Al−O bonds are formed. This is important here since the SBA silica does not present a well-ordered structure.

The calculated NMR parameters of these species can then be compared with those of the three observed sites. The most abundant observed site **S2** (δ_{iso} = 98 ppm, C_Q = 19.9 MHz) could be consistent with the structure **D2.1** (δ_{iso} = 104 ppm, C_Q = 18 MHz), while the NMR parameters of **S1** (δ_{iso} = 154 ppm, C_Q = 27.3 MHz) match structure **D2.2** (δ_{iso} = 150 ppm, C_Q = 26 MHz). The calculated η_Q values for these dimers (0.8−0.9) also agree nicely with the experimental determination for sites **S1** and **S2**. With these calculated structures, however, it is impossible to attribute **S3**.

In view of the presence of mono-, di-, and trialkylsilicon surface species, Al species bonded by more than two oxygen atoms to the surface are expected through grafting via alkyl

dx.doi.org/10.1021/ja3008566 | J. Am. Chem. Soc. 2012, 134, 6767−6775

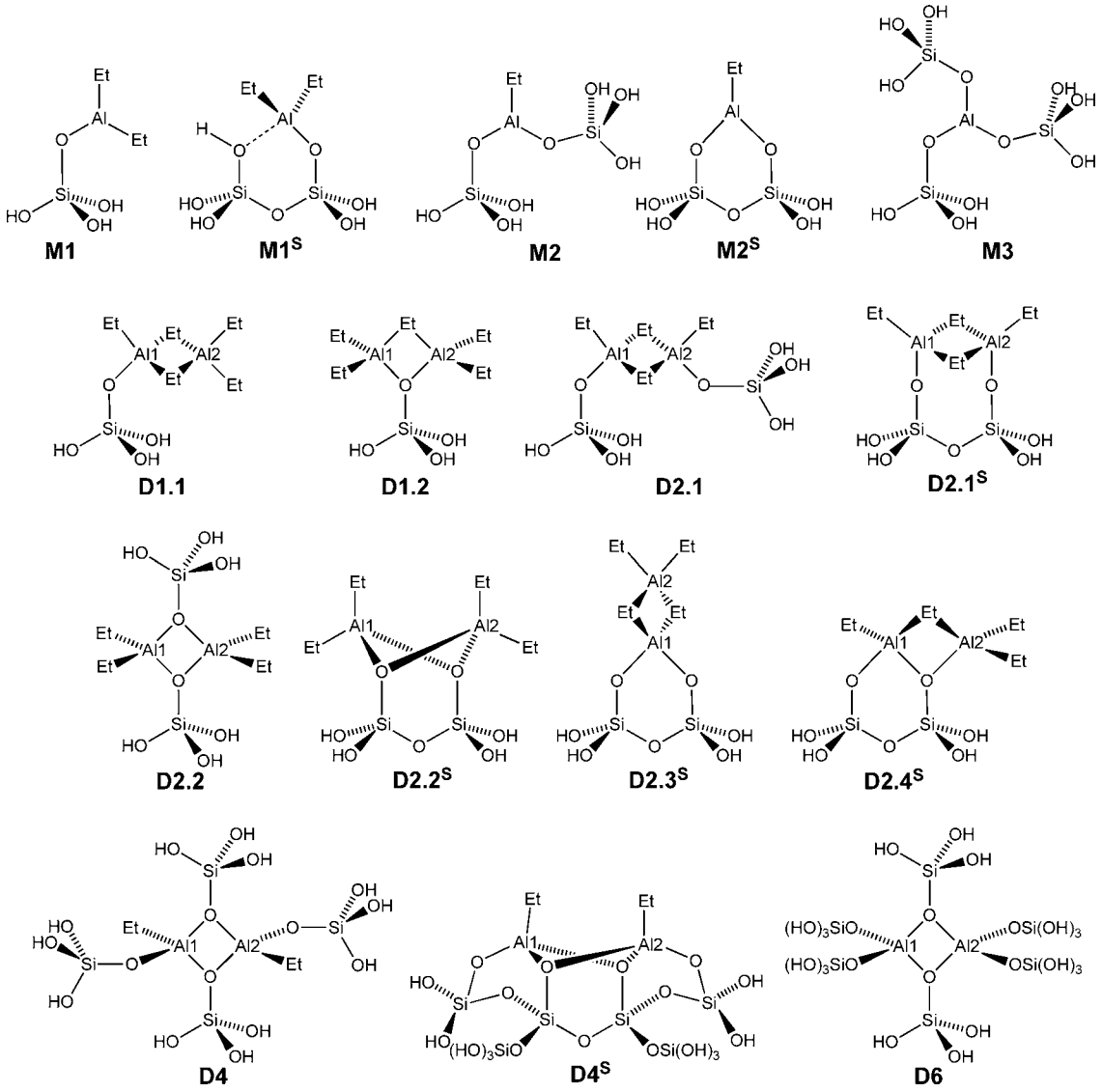

Figure 2. Models of the grafted Al species used in the calculations, either as an isolated cluster (with the terminating H atoms) or embedded on a partially dehydrated {001} surface of the β-cristobalite surface (H atoms replaced by Si atoms of the surface as shown in Figure 3).

transfer to adjacent Si−O−Si bridges (Scheme 1). As representative examples, symmetrical dimeric species having four siloxy (two bridging plus two terminal siloxy) and two alkyl groups, as in **D4**, would also display low δ_{iso} and C_Q calculated values (δ_{iso} = 90 ppm, C_Q = 21 MHz), close to the observed site **S2** (δ_{iso} = 98 ppm, C_Q = 19.9 MHz). δ_{iso} is somewhat low, at the limit of the 10 ppm error bar. **D4**^{S} is formed from **D4** by establishing three Si−O−Si links between the four Si centers. In this case of four siloxy groups, the geometry around each Al atom is more constrained than in the case of **D2.2**^{S}, and the deformation results in an increased C_Q value for the model $EtAlO_3$ species, clearly bringing it away from the experimental value. It is finally possible to surround each Al atom of the dimer by four oxygen atoms, one representative possibility being the structure **D6** (δ_{iso} = 52 ppm, C_Q = 17 MHz, η_Q = 0.5). This latter structure displays NMR parameters close to those observed for site **S3** (δ_{iso} = 60 ppm, C_Q = 15.1 MHz, η_Q = 0.4), in particular for C_Q, which is typical of the symmetric environment of tetrahedral AlO_4 species as observed for the Td site of alumina. Slight distortions in the tetrahedral geometry of AlO_4 sites could lead to significant variations for C_Q and δ_{iso} values, as observed before in the case of the γ-alumina surface,[60] zeolites,[61] or aluminosilicates,[62] and could explain the broad nature of that component in the data and the larger deviation between calculation and experiment for the chemical shift. In addition, **D6** is the only dimer species for which an intermediate value of η_Q is obtained, from the more symmetric environment.

From these cluster models, Al species on a silica surface were derived using a slab representation. The silica support was modeled by using a partially dehydrated {001} surface of β-cristobalite, with an OH coverage of 1.86 OH·nm^{-2}.[63] Although such a choice might not reflect the complex surface of the silica sample, this allows the determination of the influence of an extended surface. Calculated formation energies show that the surface grafting process on a surface OH group by protonolysis of an ethyl ligand, which results in forming an O−Al bond and an ethane molecule, is always strongly exothermic. For example, grafting by removal of a terminal ethyl group is exothermic by ∼180 kJ·mol^{-1} for mono-grafted monomers, ∼200 kJ·mol^{-1} for mono-grafted dimers, and ∼330−370 kJ·mol^{-1} for bis-grafted dimers. This is well in

dx.doi.org/10.1021/ja3008566 | J. Am. Chem. Soc. 2012, 134, 6767−6775

Table 2. Fitted Experimental ^{27}Al NMR Parameters C_Q (MHz) and δ_{iso} (ppm) for Grafted TEA on SBA and DFT-Calculated Values for Potential Structures Described as Cluster Models or Grafted on Partially Dehydrated Cristobalite (See Figure 2)

		Al1			Al2		
entry	label	$\|C_Q\|$	δ_{iso}	η_Q	$\|C_Q\|$	δ_{iso}	η_Q
		Experimental Data					
1	**S1**	27.3	154	0.8			
2	**S2**	19.9	98	0.8			
3	**S3**	15.1	60	0.4			
		TEA Monomer and Dimer					
4	Et_3Al	47	320	0.0			
5	Et_6Al_2	23	149	0.9	23	149	0.9
		Cluster Models					
6	**M1**	42	207	0.4			
7	**M2**	38	116	0.4			
8	**M3**	37	67	0.1			
9	**D1.1**	18	107	0.9	25	153	0.8
10	**D1.2**	25	151	0.8	25	152	0.8
11	**D2.1**	18	104	0.9	18	104	0.9
12	**D2.2**	26	150	0.8	26	150	0.8
13	**D2.2^S**	27	155	0.9	28	156	0.9
14	**D4**	21	90	0.9	21	90	0.9
15	**D4^S**	24	102	0.9	24	102	0.9
16	**D6**	17	52	0.5	17	52	0.5
		Grafted on Cristobalite					
17	**M1**	43	212	0.4			
18	**M1^S**	32	150	0.6			
19	**M2^S**	37	127	0.5			
20	**D1.1**	16	110	0.9	27	141	0.8
21	**D1.2**	26	153	0.8	24	147	0.8
22	**D2.1^S**	21	106	0.7	20	106	0.7
23	**D2.2^S**	28	156	0.9	28	156	0.9
24	**D2.3^S**	11	81	0.3	28	148	0.7
25	**D2.4^S**	20	111	0.8	29	153	0.8

line with the total consumption of the surface OH groups. Calculated NMR parameters for the grafted species on the cristobalite slab are given in Table 2 (lower section).

When similar structures are calculated with both the cluster and surface models (**M1**, **D1.1**, **D1.2**, and **D2.2^S**), C_Q and δ_{iso} parameters differ at maximum by 2 MHz and 12 ppm, which is smaller than the typical variation between different considered structures. The deviations are mainly related to long-range weak interactions with the surface. As a consequence, surface models confirm the previous conclusions from clusters and the relative insensitivity of the results to the detailed nature of the silica model.

The grafted monomeric species also yield high C_Q and δ_{iso} values. On the surface, a new bent structure is possible starting from **M1**, where the Al center has an additional interaction with a neighboring O atom (an OH in **M1^S**), similar to the mononuclear Al complexes grafted on silsesquioxane reported by Duchateau.[64−66] **M1^S** is 9 kJ·mol^{-1} more stable than **M1**, and the new O···Al interaction significantly weakens the C_Q and δ_{iso} values. However, the calculated C_Q for **M1^S** remains too high (32 MHz), so that such a structure cannot be associated to any experimentally observed component.

The results for the dimeric systems are also confirmed. Monografted dimers **D1.X** do not give a good agreement with the experimental data. Both Al centers in **D1.2** are roughly equivalent, and although the δ_{iso} values match the first experimental component, the C_Q component for Al_1 is too low (3.3 MHz lower than the experimental value).

As seen for the cluster models, the match with bis-grafted dimeric structures is better. Here, such systems were constructed using a selected cristobalite surface with two OH groups on neighboring Si atoms. **D2.2^S**, with two bridging siloxy ligands, gives an excellent match with the first experimental component **S1**, while **D2.1^S**, with two terminal siloxy ligands, reproduces the second component **S2** (Figure 3).

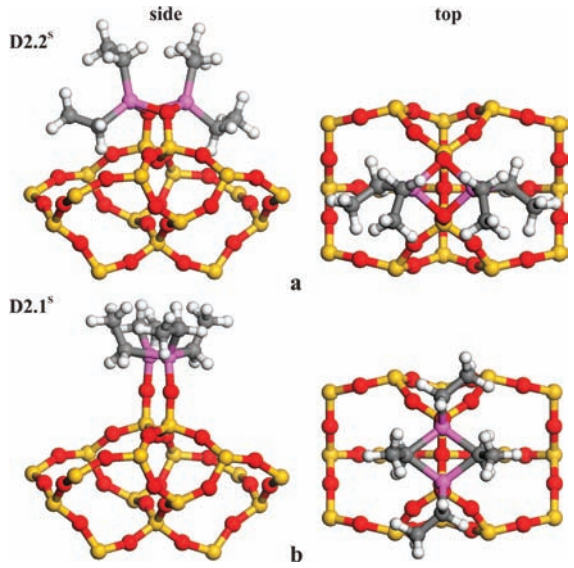

Figure 3. Proposed bis-grafted dimeric Al_2Et_4 structures obtained from the comparison between the theoretical and experimental ^{27}Al solid-state NMR data for sites **S1** (a, **D2.2^S**) and **S2** (b, **D2.1^S**). For clarity only a fragment of the {001} surface of cristobalite is shown. The Si, O, Al, C, and H atoms are presented as yellow, red, pink, gray, and white balls, respectively.

Additional possibilities were constructed. **D2.3^S** with a double terminal grafting shows a large dissymmetry between the two Al atoms, and the calculated parameters on Al_1 are consequently too low. **D2.4^S** dimer combines a terminal and a bridging siloxy ligand and is hence less dissymmetric: Al_2 is close to the parameters of **S1**, while Al_1 is close to **S2**. The calculated chemical shift for Al_1 is, however, 13 ppm larger than the fitted value for **S2**, beyond the determined error bar. The four-fold grafted **D4^S** and **D6** models were not studied on the {100} cristobalite surface, since they cannot be adapted to that specific termination.

The DFT calculations also provide the total energy of the grafted species. The general trend for mono-grafted species is that species with a bridging surface O atom (such as in **D1.2**) are ∼30 kJ·mol^{-1} more stable than those with a terminal one (such as in **D1.1**). The situation is more complex for bis-grafted species. Indeed, if the calculated NMR parameters are not significantly dependent on the distance between the two Si−O surface ligands (see above), this is not the case for the total energy, which depends on the model considered for the silica. With cluster models, grafted species with two bridging surface O atoms (such as **D2.2**) are the most stable ones, while a mixed system with bridging and terminal surface O atoms (such as **D2.4**) becomes slightly preferred on β-cristobalite. On the latter extended surface model, **D2.1^S**, **D2.2^S**, and **D2.4^S** are

dx.doi.org/10.1021/ja3008566 | J. Am. Chem. Soc. 2012, 134, 6767−6775

within 25 kJ·mol^{-1}. Hence, total energy is not a good guide in the case of a sample that does not have a well-defined surface structure.

While the current study cannot address the detailed grafting mechanism, it is possible to rationalize the results by combining the structure of the sites derived from DFT calculations and the experimental results from aluminum-27 solid-state NMR, IR, and mass balance analysis. The Al sites **S1** and **S2** are attributed to bis-grafted dimeric structures of different types: **S2**, the major site, is associated with dimeric Al species having two terminal siloxy ligands (**D2.1**^{S}), while **S1** is associated with a dimeric Al species having two bridging siloxy ligands (**D2.2**^{S}). **S2** could alternatively be assigned to the four-fold grafted **D4** structure, with only two remaining ethyl groups on the Al dimer, but this would require a grafting on a curved cavity on the surface to preserve the planar geometry of **D4**, since deformation to **D4**^{S} modifies the NMR parameters. The third Al sites **S3** correspond to tetracoordinated AlO_4 species, which shows that Al inserts into the framework of silica.[30] Considering that all OH groups are consumed during grafting of Et_6Al_2, that 1 ethane is evolved per surface OH, that there is 1.8 Al grafted per OH groups, and that there is an average of 4.6 Et per 2 Al, it is possible to propose that the major pathway of formation of these species is the grafting via a protonolysis of a single Et−Al of Et_6Al_2, followed by transfer of ethyl group(s), as this would account for the disappearance of all OH groups, the formation of 1 ethane per OH group, a resulting Al per OH group ratio of 2, and a Et per Al ratio of 5/2. The slight difference between this ideal situation and the experimental results shows that other minority routes are possible, such as grafting via protonolysis of two Et−Al bonds in Et_6Al_2; this latter pathway results in the disappearance of all OH groups and the formation of 1 ethane per OH group as well, but with a resulting Al per OH group ratio of 1 and an Et per Al ratio of 4/2. This latter pathway is not unlikely, since the OH density is not homogeneous and since the average OH coverage on SBA partially dehydroxylated at 500 °C is 1.3−1.4 OH·nm^{-2},[38] so that having 2 vicinal OH separated by 2.93 Å such as in structure **D2.1** is possible. This could explain part of the observed species such as **D2.1**. As proposed earlier, **D2.1** can also be formed by invoking alkyl transfer starting from a species such as **D1.1**. For species of structure **D2.2**, it is more likely that such species are formed by protonolysis generating **D1.2**, followed by alkyl transfer, as shown in Scheme 1. It is also noteworthy that a structure similar to **D2.2**^{S} was recently suggested upon reaction of trimethylgallium with silica according to EXAFS studies.[67] Finally, the AlO_4 species clearly results from multiple alkyl transfers; it is consistent with the species observed by silicon-29 NMR spectroscopy. Overall this difference of surface sites translates to the difference of reactivity of siloxane bridges, as expected for an amorphous support such as silica.[5]

CONCLUSION

The grafting of triethylaluminum on a mesoporous silica, here SBA-15, led to the formation of supported dimeric surface complexes as major surface species as well as integrated AlO_4 sites in silica according to the association of aluminum-27 MAS NMR spectroscopy and DFT calculations, complemented by mass balance analysis, IR spectroscopy, and silicon-29 NMR. The determination of the structures of the three observed Al sites required a detailed investigation combining aluminum-27 NMR spectroscopy at three different high magnetic fields (17.6, 20.0, and 23.5 T), using ultrafast spinning frequencies (up to 65 kHz), in combination with a computational modeling of the broad spectral lines. This spectroscopic approach was associated with DFT calculations of the geometry and NMR parameters of cluster and periodic models of the different grafted species. The approach is meaningful despite the disordered nature of the silica surface because the calculated NMR parameters do not depend significantly on the choice of the silica model. Moreover, the detailed structural analysis provided by this computational approach showed the very strong influence of the type and geometry of the Al complexes and of the nature of the Al substituents on the calculated C_Q and δ_{iso} NMR parameters, making this approach a powerful and versatile method to evaluate the structure of Al surface species. Two specific geometries for the grafted dimer, among a vast ensemble of possibilities, have been accurately determined with different positions (terminal or bridging) of the siloxy groups. The major pathway of formation of these surface Al dimers probably results from protonolysis of one Al−Et bond of Et_6Al_2, followed by alkyl transfer to an adjacent siloxane bridge. In addition, the study clearly rules out the presence of tricoordinated Al species on the silica surface, after reaction with TEA.

With this robust method in hand, we are further investigating the chemistry of aluminum complexes on oxide surfaces in the hope to have a more general understanding of the chemistry of surface alkylaluminum compounds.

METHODS

Theoretical Methods. The considered models for the grafting process of TEA (monomers and dimers) on a silica surface were computed with both cluster and periodic approaches. All calculations were performed in the framework of density functional theory (DFT) with generalized gradient approximation (GGA) exchange and correlation functionals.

Cluster Approach. All cluster calculations have been initially optimized with TURBOMOLE 6.3[68,69] using the triple-ζ def2-TZVP[70] basis set and the Perdew−Burke−Ernzerhof (PBE) functional.[71]

Periodic Approach. Periodic surface models have been optimized by using the Vienna Ab Initio Simulation Package (VASP 5.2).[72−74] The total energy is calculated with the Perdew−Wang 91 functional (PW91), which gives results that are very similar to those obtained with the PBE functional.[75,76] VASP uses plane waves complemented with the projector augmented wave (PAW) method to describe atomic cores.[72,74] For the plane wave basis set, a cutoff energy of 400 eV has been used. The silica box contains 142 atoms, with cell parameters a = b = 14.68 Å, c = 25.00 Å, $\alpha = \beta = \gamma = 90°$. From the large size of the unit cell, the Brillouin-zone sampling has been restricted to the Γ-point. The surface unit cell contains four silanol groups (−OH), which corresponds to an OH coverage of 1.86 OH·nm^{-2}, as mentioned earlier. The relaxations were stopped when the changes in the gradients of the energy were smaller than 0.01 eV·Å^{-1}.

^{27}Al NMR Calculations. The NMR parameters, chemical shifts (δ_{iso}), and quadrupolar coupling constants (C_Q) for both cluster and periodic models were calculated using the gauge-including projector augmented wave (GIPAW) method,[77] as implemented in the CASTEP 5.0 code.[78] An energy cutoff of 490 eV was employed, and calculations were performed at the Γ-point. The chemical shift calculations were referenced by using bulk α-Al_2O_3 (σ_{REF} = 532 ppm, δ_{isoREF} = 10 ppm). For the cluster models, the geometry was reoptimized within CASTEP to be fully consistent. For the periodic models, detailed tests have shown that reoptimization is completely unnecessary, since it leads to fully negligible changes in the calculated NMR parameters.

Experimental Methods. *General Information.* The grafting reaction was carried out under an argon atmosphere using dried

dx.doi.org/10.1021/ja3008566 | J. Am. Chem. Soc. 2012, 134, 6767−6775

and freshly distilled solvents. Tetraethoxysilane (TEOS), pluronic P123, pentane, and TEA solution (1 M in hexane) were purchased from Sigma-Aldrich. Mesoporous SBA-15 was synthesized following the procedure previously reported in the literature.[79] Titration of surface OH groups after thermal treatment (vide infra) was performed by contacting SBA with methylmagnesium bromide and measuring the amount of evolved methane.

Elemental analyses were performed at Mikroanalytisches Labor Pascher. Gas chromatographic analyses were performed on a Agilent 7890A GC system using an Agilent 19091P-K15 column (50 m, 0.32 mm diameter, 0.8 μm film thickness). Infrared spectra (DRIFT) were recorded on a Nicolet Magna 6700 FT spectrometer equipped with a cell under a controlled atmosphere.

Preparation of the Grafted Materials TEA@SBA-15. Under an inert atmosphere, to 0.523 g of SBA-15 pretreated under high vacuum (1×10^{-5} mbar) conditions at 500 °C for 12 h was added 2.0 mL of TEA solution (2.0 mmol) diluted in 10.0 mL of dry and degassed pentane, using the double Schlenk technique. After 2 h at room temperature, the material was filtered. To wash the solid, the pentane of the TEA solution was evaporated and condensed on the solid with liquid nitrogen. This manipulation was repeated three times to remove unreacted TEA. All volatiles were evacuated into a 10 L flask. These compounds were analyzed by GC to determine the concentration of ethane formed during the grafting. The solid was transferred into a Schlenk tube using a glovebox and dried under high vacuum (1×10^{-5} mbar) for 1 h. Ethane concentration: 1.47 mmol/$g_{SBA\text{-}15}$. Elemental analysis: C, 11.62; H, 2.44; Al, 5.69.

DRIFT (4000−650 cm^{-1}): stretching C−H vibrations, 2949, 2910, 2873 cm^{-1}; bending C−H vibrations, 1463, 1411, 1380 cm^{-1}.

High Magnetic Field Aluminum-27 Solid-State NMR Spectroscopy. The ^{27}Al rotor-synchronized Hahn-echo experiment was performed on Bruker Avance III Wide Bore 750 (17.6 T) and 850 (20.0 T) and Standard Bore 1000 (23.5 T) spectrometers operating at ^{27}Al frequencies of 195.5, 221.6, and 260.7 MHz, respectively. The sample was packed in a 1.3 mm zirconia rotor inside an argon-filled glovebox and then spun between 62 and 65 kHz using pure nitrogen gas and a controlled temperature of ∼30 °C (real sample temperature). The full echo was acquired after 33 rotor periods (i.e., 500 μs), with no obvious changes in the line shape being observed by varying the echo delay up to this point. The ^{27}Al rf field was set to 50 kHz for all experiments. At 17.6 T, a "T_{90}" pulse of 1.25 μs was used, that is, slightly below the expected selective $\pi/2(I + {}^1/_2)$ value to increase the irradiation bandwidth while minimizing sensitivity losses, whereas a 1.67 μs T_{90} was used at 20.0 and 23.5 T since lowering this value led to a too-important decrease of the signal intensity. A recycle delay of 1 s was set, and 150 000 (17.6 T), 82 000 (20.0 T), and 65 000 (23.5 T) scans were accumulated. The full echo acquisition and processing ensures an unambiguous processing, a flat baseline, and a proper selection of the central transition of ^{27}Al. The MQMAS experiment was performed at 20.0 T using a z-filter sequence[80] and rf fields of 400 kHz for excitation and reconversion (pulses of 1.8 and 0.5 μs, respectively) and 50 kHz for selective T_{90}. The same conditions were used at 23.5 T, except that the rf field was 340 kHz for the triple-quantum excitation and reconversion (pulses of 1.2 and 0.5 μs, respectively). At 20.0 or 23.5 T, respectively, we used recycle delays of 0.25 or 0.5 s, and 57 600 or 14 400 transients were accumulated for each slice of the hypercomplex indirect acquisition, which consisted of 17 or 24 t_1 points with a synchronized spectral width[81] of half of the spinning speed. All spectra are externally referenced to a 1 M solution of aluminum nitrate.

■ ASSOCIATED CONTENT

Supporting Information

Infrared spectrum of TEA@SBA-15; additional NMR spectroscopy experimental details; solid-state $\{^1H\}^{29}Si$ CP-MAS NMR spectrum and solid-state $\{^1H\}^{13}C$ CP-MAS NMR spectrum of TEA@SBA-15; nitrogen adsorption/desorption experimental procedure; reference calculations performed for well-defined compounds with different Al sites (Al^{IV}, Al^{V}, Al^{VI}); structure of the unit cell for the selected {001} surface of cristobalite. This material is available free of charge via the Internet at http://pubs.acs.org.

■ AUTHOR INFORMATION

Corresponding Author

philippe.sautet@ens-lyon.fr

Present Addresses

[⊗]Department of Chemistry, ETH Zürich, Wolfgang-Pauli Strasse 10, CH-8093 Zürich, Switzerland.

[▽]Materials Design, 18 rue de Saisset, F-92120 Montrouge, France.

Notes

The authors declare no competing financial interest.

■ ACKNOWLEDGMENTS

This publication is based on work supported by Award No. UK-C0017, made by King Abdullah University of Science and Technology (KAUST), and by the TGE RMN THC Fr3050. The authors thank the PSMN at ENS of Lyon for the attribution of CPU time and Raphael Wischert for sharing data (ref 60).

■ REFERENCES

(1) Hlatky, G. G. *Chem. Rev.* **2000**, *100*, 1347−1376.
(2) Corma, A.; Garcia, H. *Chem. Rev.* **2002**, *102*, 3837−3892.
(3) Copéret, C.; Chabanas, M.; Petroff Saint-Arroman, R.; Basset, J.-M. *Angew. Chem., Int. Ed.* **2003**, *42*, 156−181.
(4) Thomas, J. M.; Raja, R.; Lewis, D. W. *Angew. Chem., Int. Ed.* **2005**, *44*, 6456−6482.
(5) Gajan, D.; Copéret, C. *New J. Chem.* **2011**, *35*, 2403−2408.
(6) Saito, S.; Yamamoto, H. *Chem. Commun.* **1997**, 1585−1592.
(7) Corma, A.; Garcia, H. *Chem. Rev.* **2003**, *103*, 4307−4365.
(8) Taguchi, T.; Yanai, H. In *Acid Catalysis in Modern Organic Synthesis*; Yamamoto, H., Ishihara, K., Eds.; Wiley-VCH: Weinheim, 2008; Vol. *1*, pp 241−345.
(9) Hunger, M. In *Zeolites and Catalysis*; Cejka, J., Corma, A., Zones, S., Eds.; Wiley-VCH: Weinheim, 2010; Vol. *2*, pp 493−546.
(10) Severn, J. R.; Chadwick, J. C.; Duchateau, R.; Friederichs, N. *Chem. Rev.* **2005**, *105*, 4073−4147.
(11) Chen, E. Y.-X.; Marks, T. J. *Chem. Rev.* **2000**, *100*, 1391−1434.
(12) Sinn, H.; Kaminsky, W.; Vollmer, H. J.; Woldt, R. *Angew. Chem.* **1980**, *92*, 396−402.
(13) Zurek, E.; Ziegler, T. *Prog. Polym. Sci.* **2004**, *29*, 107−148.
(14) Negureanu, L.; Hall, R. W.; Butler, L. G.; Simeral, L. A. *J. Am. Chem. Soc.* **2006**, *128*, 16816−16826.
(15) Linnolahti, M.; Severn, J. R.; Pakkanen, T. A. *Angew. Chem., Int. Ed.* **2008**, *47*, 9279−9283.
(16) Glaser, R.; Sun, X. *J. Am. Chem. Soc.* **2011**, *133*, 13323−13336.
(17) Köppl, A.; Alt, H. G.; Schmidt, R. *J. Organomet. Chem.* **1999**, *577*, 351−357.
(18) Hammawa, H.; Wanke, S. E. *J. Appl. Polym. Sci.* **2007**, *104*, 514−527.
(19) Sano, T.; Doi, K.; Hagimoto, H.; Wang, Z.; Uozumi, T.; Soga, K. *Chem. Commun.* **1999**, 733−734.
(20) Van Looveren, L. K.; Geysen, D. F.; Vercruysse, K. A.; Wouters, B. H.; Grobet, P. J.; Jacobs, P. A. *Angew. Chem., Int. Ed.* **1998**, *37*, 517−520.
(21) Camposa, J. M.; Ribeiro, M. R.; Lourenço, J. P.; Fernandes, A. *J. Mol. Catal. A* **2007**, *277*, 93−101.
(22) Peglar, R. J.; Hambleton, F. H.; Hockey, J. A. *J. Catal.* **1971**, *20*, 309−320.
(23) Low, M. J. D.; Severdia, A. G.; Chan, J. *J. Catal.* **1981**, *69*, 384−391.

(24) Anwander, R.; Palm, C.; Groeger, O.; Engelhardt, G. *Organometallics* **1998**, *17*, 2027−2036.
(25) Blitz, J. P.; Diebel, R. E.; Deakyne, C. A.; Christensen, J. M.; Gun'ko, V. M. *J. Phys. Chem. B* **2005**, *109*, 5667−5677.
(26) Scott, S. L.; Church, T. L.; Nguyen, D. H.; Mader, E. A.; Moran, J. *Top. Catal.* **2005**, *34*, 109−120.
(27) Li, J.; DiVerdi, J. A.; Maciel, G. E. *J. Am. Chem. Soc.* **2006**, *128*, 17093−17101.
(28) Pelletier, J.; Espinas, J.; Vu, N.; Norsic, S.; Baudouin, A.; Delevoye, L.; Trébosc, J.; Roux, E. L.; Santini, C.; Basset, J.-M.; Gauvin, R. M.; Taoufik, M. *Chem. Commun.* **2011**, *47*, 2979−2981.
(29) Kwak, J. H.; Hu, J.; Mei, D.; Yi, C.-W.; Kim, D. H.; Peden, C. H. F.; Allard, L. F.; Szanyi, J. *Science* **2009**, *325*, 1670−1673.
(30) Smith, M. E. *Appl. Magn. Reson.* **1993**, *4*, 1−64.
(31) Jianga, Y.; Huangb, J.; Daic, W.; Hunger, M. *Solid State Nucl. Magn. Reson.* **2011**, *39*, 116−141.
(32) Skibsted, J.; Bildsøe, H.; Jakobsen, H. J. *J. Magn. Reson.* **1991**, *92*, 669−676.
(33) Massiot, D.; Fayon, F.; Deschamps, M.; Cadars, S.; Florian, P.; Montouillout, V.; Pellerin, N.; Hiet, J.; Rakhmatullin, A.; Bessada, C. *C. R. Chim.* **2010**, *13*, 117−129.
(34) Bryant, P. L.; Butler, L. G.; Reyes, A. P.; Kuhns, P. *Solid State Nucl. Magn. Reson.* **2000**, *16*, 63−67.
(35) Bräuniger, T.; Chandran, C. V.; Wedig, U.; Jansen, M. *Z. Anorg. Allg. Chem.* **2011**, *637*, 530−535.
(36) Jerschow, A. *Prog. Nucl. Magn. Reson. Spectrosc.* **2005**, *46*, 63−78.
(37) Zhao, D.; Feng, J.; Huo, Q.; Melosh, N.; Fredrickson, G. H.; Chmelka, B. F.; Stucky, G. D. *Science* **1998**, *279*, 548−552.
(38) Zhuravlev, L. T. *Colloids Surf., A* **2000**, *173*, 1−38.
(39) Panchenko, V. N.; Zakharov, V. A.; Danilova, I. G.; Paukshtis, E. A.; Zakharov, I. I.; Goncharov, V. G.; Suknev, A. P. *J. Mol. Catal. A* **2001**, *174*, 107−117.
(40) Gizbar, H.; Vestfrid, Y.; Chusid, O.; Gofer, Y.; Gottlieb, H. E.; Marks, V.; Aurbach, D. *Organometallics* **2004**, *23*, 3826−3831.
(41) Le Caër, G.; Brand, R. A. *J. Phys. Condens. Matter* **1998**, *10*, 10715−10774.
(42) Neuville, D. R.; Cormier, L.; Massiot, D. *Geochim. Cosmochim. Acta* **2004**, *68*, 5071−5079.
(43) Le Caër, G.; Bureau, B.; Massiot, D. *J. Phys. Condens. Matter* **2010**, *22*, 065402.
(44) Massiot, D.; Fayon, F.; Capron, M.; King, I.; Le Calvé, S.; Alonso, B.; Durand, J.-O.; Bujoli, B.; Gan, Z.; Hoatson, G. *Magn. Reson. Chem.* **2002**, *40*, 70−76.
(45) The DMFit program has been modified to account for this model and is available on request.
(46) Mason, M. R.; Smith, J. M.; Bott, S. G.; Barron, A. R. *J. Am. Chem. Soc.* **1993**, *115*, 4971−4984.
(47) Healy, M. D.; Power, M. B.; Barron, A. R. *Coord. Chem. Rev.* **1994**, *130*, 63−135.
(48) Barron, A. R. *Polyhedron* **1995**, *14*, 3197−3207.
(49) Cottone, A.; Scott, M. J. *Organometallics* **2002**, *21*, 3610−3627.
(50) Son, A. J. R.; Thorn, M. G.; Fanwick, P. E.; Rothwell, I. P. *Organometallics* **2003**, *22*, 2318−2324.
(51) Wrobel, O.; Schaper, F.; Brintzinger, H. H. *Organometallics* **2004**, *23*, 900−905.
(52) McGrady, G. S.; Turner, J. F. C.; Ibberson, R. M.; Prager, M. *Organometallics* **2000**, *19*, 4398−4401.
(53) Klosin, J.; Roof, G. R.; Chen, E. Y.-X.; Abboud, K. A. *Organometallics* **2000**, *19*, 4684−4686.
(54) Cottone, A.; Scott, M. J. *Organometallics* **2000**, *19*, 5254−5256.
(55) Benn, R.; Janssen, E.; Lehmkuhl, H.; Rufińska, A. *J. Organomet. Chem.* **1987**, *333*, 155−168.
(56) Yates, D. J. C.; Dembinski, G. W.; Kroll, W. R.; Elliott, J. J. *J. Phys. Chem.* **1969**, *73*, 911−921.
(57) Apblett, A. W.; Barron, A. R. *Organometallics* **1990**, *9*, 2137−2141.
(58) Mulhaupt, R.; Calabrese, J.; Ittel, S. D. *Organometallics* **1991**, *10*, 3403−3406.
(59) McMahon, C. N.; Bott, S. G.; Alemany, L. B.; Roesky, H. W.; Barron, A. R. *Organometallics* **1999**, *18*, 5395−5408.
(60) Wischert, R.; Copéret, C.; Florian, P.; Delbecq, F.; Sautet, P. Unpublished results.
(61) Sklenak, S.; Dědeček, J.; Li, C.; Wichterlová, B.; Gábová, V.; Sierka, M.; Sauer, J. *Phys. Chem. Chem. Phys.* **2009**, *11*, 1237−1247.
(62) Lippmaa, E.; Samoson, A.; Mägi, M. *J. Am. Chem. Soc.* **1986**, *108*, 1730−1735.
(63) Rozanska, X.; Delbecq, F.; Sautet, P. *Phys. Chem. Chem. Phys.* **2010**, *12*, 14930−14940.
(64) Duchateau, R.; Harmsen, R. J.; Abbenhuis, H. C. L.; Santen, R. A. v.; Meetsma, A.; Thiele, S. K.-H.; Kranenburg, M. *Chem.—Eur. J.* **1999**, *5*, 3130−3135.
(65) Skowronska-Ptasinska, M. D.; Duchateau, R.; van Santen, R. A.; Yap, G. P. A. *Organometallics* **2001**, *20*, 3519−3530.
(66) Duchateau, R. *Chem. Rev.* **2002**, *102*, 3525−3542.
(67) Fleischman, S. D.; Scott, S. L. *J. Am. Chem. Soc.* **2011**, *133*, 4847−4855.
(68) *TURBOMOLE*, V6.3 2011; a development of the University of Karlsruhe and Forschungszentrum Karlsruhe GmbH; 1989−2007; TURBOMOLE GmbH, since 2007; available from http://www.turbomole.com.
(69) Ahlrichs, R.; Bär, M.; Häser, M.; Horn, H.; Kölmel, C. *Chem. Phys. Lett.* **1989**, *162*, 165−169.
(70) Rappoport, D.; Furche, F. *J. Chem. Phys.* **2010**, *133*, 134105.
(71) Perdew, J. P.; Burke, K.; Ernzerhof, M. *Phys. Rev. Lett.* **1996**, *77*, 3865−3868.
(72) Blöchl, P. E. *Phys. Rev. B* **1994**, *50*, 17953−17979.
(73) Kresse, G.; Furthmüller, J. *Comput. Mater. Sci.* **1996**, *6*, 15−50.
(74) Kresse, G.; Joubert, D. *Phys. Rev. B* **1999**, *59*, 1758−1775.
(75) Perdew, J. P.; Chevary, J. A.; Vosko, S. H.; Jackson, K. A.; Pederson, M. R.; Singh, D. J.; Fiolhais, C. *Phys. Rev. B* **1992**, *46*, 6671−6687.
(76) Perdew, J. P.; Chevary, J. A.; Vosko, S. H.; Jackson, K. A.; Pederson, M. R.; Singh, D. J.; Fiolhais, C. *Phys. Rev. B* **1993**, *48*, 4978−4978.
(77) Pickard, C. J.; Mauri, F. *Phys. Rev. B* **2001**, *63*, 245101.
(78) Clark, S. J.; Segall, M. D.; Pickard, C. J.; Hasnip, P. J.; Probert, M. I. J.; Refson, K.; Payne, A. M. C. *Z. Kristallogr.* **2005**, *220*, 567−570.
(79) Zhao, D.; Huo, Q.; Feng, J.; Chmelka, B. F.; Stucky, G. D. *J. Am. Chem. Soc.* **1998**, *120*, 6024−6036.
(80) Amoureux, J.-P.; Fernandez, C.; Steuernagel, S. *J. Magn. Reson., Ser. A* **1996**, *123*, 116−118.
(81) Massiot, D. *J. Magn. Reson., Ser. A* **1996**, *122*, 240−244.